Volume 26
Number 23
21 June 2024
Pages 3007–3132

CrystEngComm

rsc.li/crystengcomm

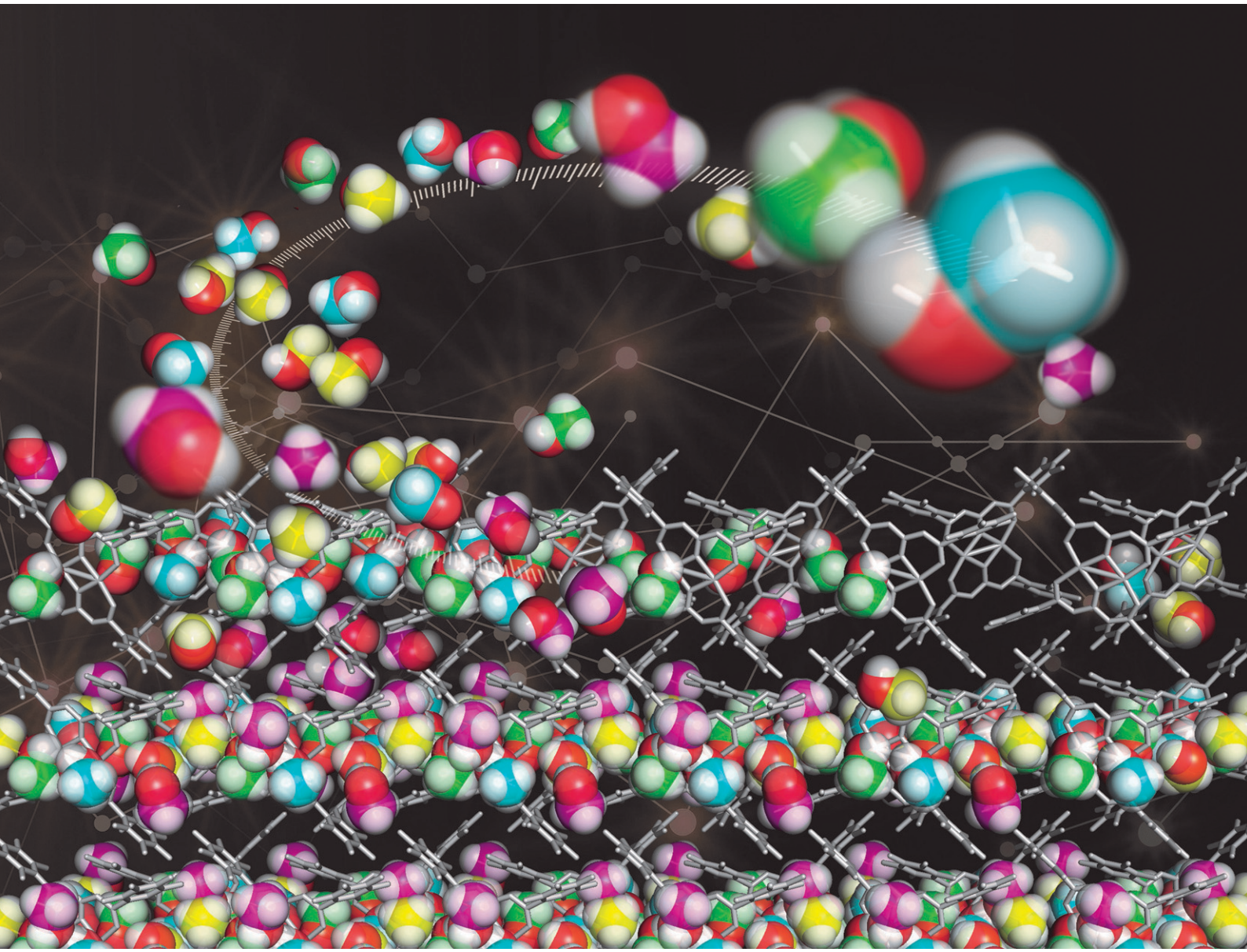

ISSN 1466-8033

ROYAL SOCIETY OF CHEMISTRY

COMMUNICATION

Akiko Hori *et al.*

Selective recognition and reversible encapsulation of tetrameric alcohol clusters *via* hydrogen bonds using a perfluorinated dinuclear nickel(II) complex

CrystEngComm

ROYAL SOCIETY OF CHEMISTRY

COMMUNICATION

View Article Online
View Journal | View Issue

Cite this: *CrystEngComm*, 2024, **26**, 3014

Received 23rd February 2024,
Accepted 10th May 2024

DOI: 10.1039/d4ce00166d

rsc.li/crystengcomm

Selective recognition and reversible encapsulation of tetrameric alcohol clusters *via* hydrogen bonds using a perfluorinated dinuclear nickel(II) complex†

Yusuke Habuka,[a] Hirotomo Usui,[a] Mizuki Okawa,[a] Takanori Shinohara,[b] Hidetaka Yuge,[b] Yuchen Mao,[c] Jin Gong,[c] Gary J. Richards[a] and Akiko Hori *[a]

Perfluorinated dinuclear metal complexes, $[M_2L_2]$ (M = Ni^{2+} (1), Cu^{2+} (2), and H_2L = 1,5-dihydroxy-1,5-bis(pentafluorophenyl)-1,4-pentadien-3-one), were examined as host crystals to encapsulate alcohol molecules. Complex 1 was crystallized from EtOH and MeOH to give unique single crystals 1·2EtOH·2H_2O and 1·8MeOH, respectively, showing a unique hydrogen bonded motif of solvent molecules due to the hydrophobic crystalline cavities surrounded by the pentafluorophenyl moieties on the dinuclear Ni^{2+} sites. This open and specific cavity on the metals is not suitable for EtOH or H_2O in the crystallization process whereas MeOH, a physiologically harmful substance used in industry, is effectively and selectively encapsulated. The encapsulated MeOH molecules form tetrameric clusters that are stabilized by hydrogen bonding. Vapor adsorption of the powder samples shows reversible and accelerated recognition of alcohol only for the perfluorinated complex 1, while two coordination solvates were observed for 2.

Guest inclusion can transform the crystal shapes of host materials along with their corresponding physical properties based on their structure, intriguing many researchers who work in the fields of material science and organic and coordination chemistries.[1–4] The driving force for reversible capturing of guest molecules is governed by weak interactions,[5,6] *e.g.*, hydrogen bonding, coordination bonding, and aromatic stacking, that are based on dipole and quadrupole moments.[7–9] The design of weak interactions for functional groups is particularly important in the creation of new solid state host materials. The design of host materials using molecular crystals and low-dimensional integrated metal complexes requires clear and specific molecular design in order to change the cavity space according to the guest. It also requires visualization of affinity with the guest molecules and their intermolecular interactions.[10–12] The reversible adsorption of aromatic guest molecules with concurrent color and shape changes of non-porous host crystals of fully fluorinated metal complexes was previously achieved, and the driving force of the guest insertion process was demonstrated to be a result of the formation of hydrophobic pockets surrounded by pentafluorophenyl groups.[13–15] In particular, it has been found that Cu^{2+} complexes form several pseudo-polymorphic crystals incorporating benzene derivatives though enhanced intermolecular metal$\cdots\pi$[13,16,17] and π-hole$\cdots\pi$ interaction.[18–20]

In this study, we focused on methanol, which is industrially important as a synthetic raw material for phenolic resins and adhesives,[21,22] and is used as a solvent for various chemical reactions.[23] Although methanol is an extremely versatile and convenient solvent there are concerns regarding its toxicity,[24] and a method of recognition and separation of MeOH from similar polarity compounds such as EtOH and H_2O is required.[25] These backgrounds prompted us to investigate a Ni^{2+} complex that (a) can switch its coordination geometry between hexa-coordinated octahedral and tetra-coordinated planar, (b) can form co-crystals with guest inserted cavities at the axial position of the Ni^{2+} ions, and (c) exhibit reversible and enhanced insertion behavior of alcohol compounds. Thus, as a development of host crystals that include solvent molecules, we synthesized a dinuclear Ni^{2+} complex (1) using the pentafluorophenyl-substituted triketonate ligand, H_2L,[26] to help understand the intermolecular interactions between the complex and alcohol molecules (Scheme 1). Complex 1 gives unique crystals 1·2EtOH·2H_2O and 1·8MeOH from solutions of EtOH and MeOH, respectively. In the crystal of 1·8MeOH, two clusters of tetrameric MeOH were formed on the two

[a] *Graduate School of Engineering and Science, Shibaura Institute of Technology, Fukasaku 307, Minuma-ku, Saitama 337-8570, Japan.*
E-mail: ahori@shibaura-it.ac.jp; Fax: +81 48 687 5013; Tel: +81 48 720 6350
[b] *Department of Chemistry, School of Science, Kitasato University, Kitasato 1-15-1, Minami-ku, Sagamihara 252-0373, Japan*
[c] *Graduate School of Organic Materials Science, Yamagata University, Jonan 4-3-16, Yonezawa, Yamagata 992-8510, Japan*

† Electronic supplementary information (ESI) available: Crystallographic, Hirshfeld surface, DFT analysis and the corresponding nickel complexes with alcohol molecules were summarized. CCDC 1914680–1914683. For ESI and crystallographic data in CIF or other electronic format see DOI: https://doi.org/10.1039/d4ce00166d

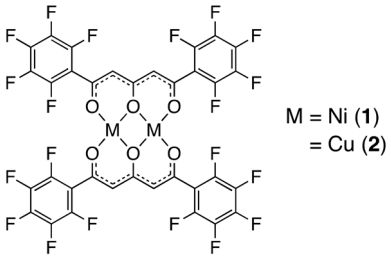

Scheme 1 Molecular structures of the complexes, **1** and **2**.

axial positions of the complex and reversible and accelerated MeOH insertion processes are found from adsorption studies indicating the formation of an alcohol cluster through intermolecular hydrogen bonds. The alcohol encapsulation behavior of powdered **1** and of distributed states of **1** in a polymer matrix, consisting of a gel membrane using a T-SMG (transparent shape memory gel),[27–29] were performed to gain understanding of the guest inclusion behaviours and for development of sensor materials for MeOH. The comparative studies of Cu^{2+} complex **2** are also performed to show specificity of the hydrogen-bonding forms for **1**.

Complex **1** was prepared from $Ni(OAc)_2{\cdot}4H_2O$ and H_2L (ref. 26) in a 68% yield. Typically, to a solution of H_2L (0.5 mmol) in MeOH (10 mL), a solution of $Ni(OAc)_2{\cdot}4H_2O$ (0.5 mmol) in MeOH (5 mL) was added. The reaction mixture was stirred for 3 h at r.t., then the solvent was removed. The residue was extracted with CH_3COOEt and dried at 100 °C for 2 h to give a brown powder. The result of elemental analysis shows good agreements of the complex **1**: calcd. for $C_{34}H_4Ni_2F_{20}O_6$ (%): C 40.60, H 0.40; found: C 40.21, H 0.50.

Crystals suitable for single-crystallographic X-ray analysis, were prepared by slow evaporation of an EtOH solution under ambient conditions to give green prismatic crystals of **1**·2EtOH·2H_2O. The asymmetric unit of the crystal contains one half of the complex, one EtOH (O4–C18–C19), and one H_2O (O5) and the whole complex which is centrosymmetric and comprises two Ni^{2+} ions, two ligands (L^{2-}), two EtOH, and two H_2O molecules to give the dinuclear nickel complex as shown in Fig. 1. The geometries around the metal center are pseudo octahedral and the metal···metal separations are 3.0465(5) Å. The bond distances of Ni–O1, Ni–O2, Ni–$O2^i$, Ni–$O3^i$ (i: $-x+1, -y+1, -z+1$) are 1.9839(14), 2.0146(14), 1.9909(13), 2.0036(14) Å, respectively, and the EtOH and H_2O molecules are coordinated at axial sites of Ni^{2+} ions, and the bond distances of Ni–O4(EtOH) and Ni–O5(H_2O) are 2.0829(16), and 2.1314(16) Å, respectively. A unique hydrogen bonded motif was observed between the coordinated EtOH and H_2O molecules (Table 1). Crystallization was performed from commercially available EtOH (99%), which was used without further purification, to give the preferential EtOH and H_2O coordinated form, indicating that the H_2O contained in the solvent or air facilitate the crystal growth. The pentafluorophenyl groups are twisted with respect to the coordination plane and the corresponding dihedral angles of the rings-A and B from the coordination plane are 40.33° and 31.31°, respectively.

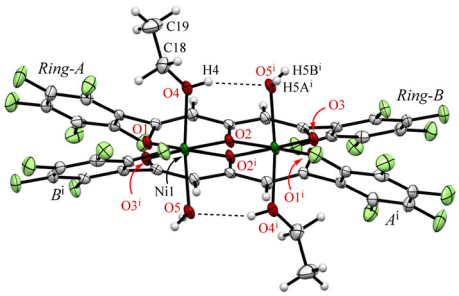

Fig. 1 The molecular structure of **1**·2EtOH·2H_2O at 103 K, showing the atom-labelling schemes. Displacement ellipsoids are drawn at the 50% probability level. Symmetry code: (i) $-x+1, -y+1, -z+1$.

On the other hand, greenish yellow block single crystals of **1**·8MeOH were obtained from slow evaporation of a MeOH solution of **1**. The asymmetric unit of the crystal contains one half of the complex and four MeOH molecules (MeOH-***a***–***d***) indicating high affinity of MeOH for the complex as shown in Fig. 2. The geometries around the metal center are pseudo octahedral. The intramolecular metal···metal separation is slightly expanded, 3.1229(4) Å, and the bond distances of Ni–O1, Ni–O2, Ni–$O2^i$, and Ni–$O3^i$ are similar to **1**·2EtOH·2H_2O. For the coordinated MeOH molecules at the axial sites of Ni^{2+} ions, the bond distances of Ni–O4 (MeOH-***a***) and Ni-O5 (MeOH-***b***) are 2.100(2) and 2.081(2) Å, respectively. On the axial sites, two clusters of four MeOH molecules are observed through three-types of hydrogen bonds in the asymmetric unit (Table 2): *i.e.*, $O4^i$–$H4^i$···O6, O5–H5···O6, and O6–H6···O7 bonds centered around MeOH-***c*** surrounded by chelated hydrogen bonds. The hydrogen (H7) of the terminal MeOH-***d*** is further interacted to the oxygen (O3) of the complex.

Since Ni^{2+} and Cu^{2+} ions have the electrophilic characteristic to coordinate lone pairs, such as alcohols, numerous corresponding solvated crystals have been reported in CSD (ver. 2024.1.0), *e.g.*, 988 and 1104 examples for MeOH included NiO_4 and CuO_4 cores, respectively. However, the eight MeOH molecules for two Ni^{2+} ions reported here is a significantly higher encapsulation ratio than previously reported to the best of our knowledge. It should be noted that there were only 27 and 9 examples of high MeOH-containing crystals (≥4 molecules per metal) for CuO_4 and NiO_4 core, respectively (see ESI† S5). However, there were no cases of similar assembling tetrameric clusters to this example in which the formation of MeOH

Table 1 Short hydrogen intermolecular contacts for **1**·2EtOH·2H_2O: donor (D) and acceptor (A)

D–H···A[a]	D–H (Å)	H···A (Å)	D···A (Å)	D–H···A (°)
O4–H4···$O5^i$	0.75(3)	2.10(3)	2.820(2)	160(3)
O5–H5A···$O3^{ii}$	0.79(3)	2.26(3)	2.948(2)	146(3)
O5–H5B···$O1^{iii}$	0.86(3)	1.80(3)	2.614(2)	158(3)

[a] Symmetric operations: (i) $-x+1, -y+1, -z+1$, (ii) $x, y-1, z$, (iii) $-x+1, -y, -z+1$.

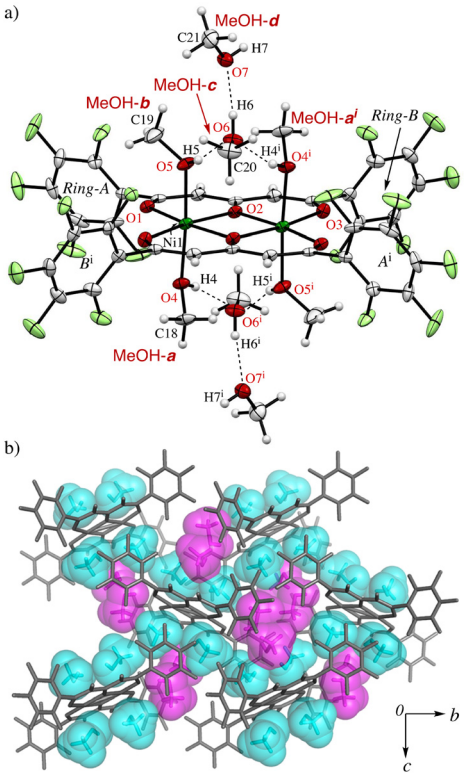

Fig. 2 a) The molecular structure of **1**·8MeOH at 93 K, showing the atom-labelling schemes. Displacement ellipsoids are drawn at the 50% probability level. b) Supramolecular association of MeOH molecules in the crystal. Color schemes: gray and cylinder structure, **1**; blue, coordinated MeOH-***a*** and -***b***; pink, solvated MeOH-***c*** and -***d***.

Table 2 Short hydrogen intermolecular contacts for **1**·8MeOH: donor (D) and acceptor (A)

D–H···A[a]	D–H (Å)	H···A (Å)	D···A (Å)	D–H···A (°)
O4–H4···O6^{i}	0.82(3)	1.98(3)	2.760(3)	161(4)
O5–H5···O6	0.79(4)	1.92(4)	2.697(3)	166(3)
O6–H6···O7	0.82(3)	1.82(3)	2.629(3)	170(3)
O7–H7···O3^{iv}	0.79(3)	1.93(3)	2.712(3)	170(3)

[a] Symmetric operations: (i) $-x+1, -y+1, -z+1$, (iv) $x, -y+3/2, z+1/2$.

clusters occurred spontaneously, the structures only occur in the following cases; 1) where MeOH molecules can highly coordinate to the coordination sites of Ni^{2+} or 2) where MeOH and/or H_2O can be filled in the preserved internal spaces in the crystalline states.[30–33] The pentafluorophenyl groups are highly twisted with respect to the coordination rings and the dihedral angles of the rings-A and B from the coordination plane are 70.60° and 72.29°, respectively, to give unique hydrophobic cavities with MeOH molecules surrounded by the perfluorinated groups. Therefore, the twisted formation of the pentafluorophenyl groups play guest adjustment functions. Part of the crystal packing structure of **1**·8MeOH is shown in Fig. 2b and 3b, showing the high ordered network between the coordinated and the solvated MeOH molecules.

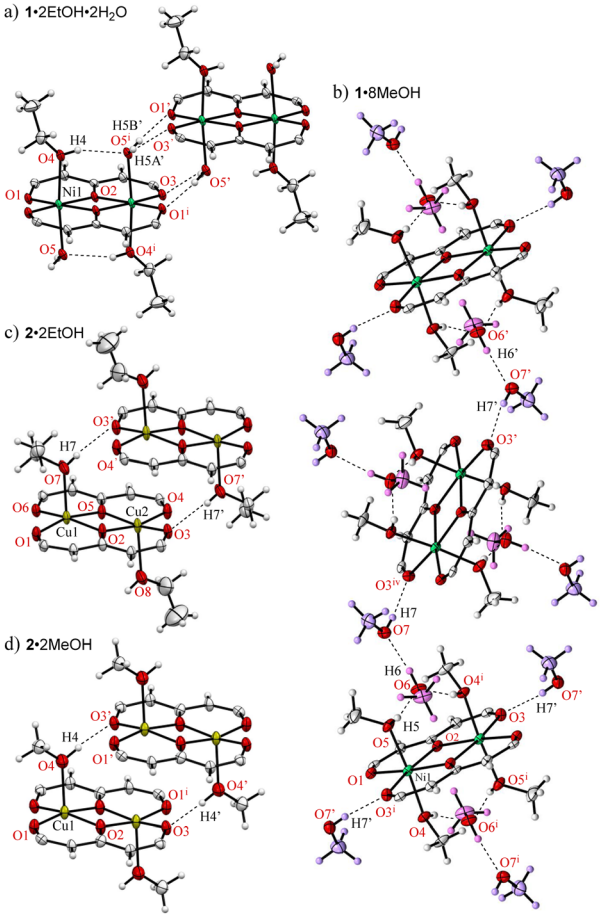

Fig. 3 A part of packing structures of a) **1**·2EtOH·2H_2O, b) **1**·8MeOH, c) **2**·2EtOH, and d) **2**·2MeOH through intra and intermolecular hydrogen bonds of MeOH. Displacement ellipsoids are drawn at the 50% probability level. The pentafluorophenyl groups of ligands were omitted.

The crystal structures of the corresponding Cu^{2+} complex **2**, which were prepared using a previously reported protocol,[15,26] from EtOH and MeOH show coordinated alcohols but the number of molecules and the coordination geometries are different to those found using the same protocols for the crystallization of **1**; *i.e.*, brown crystals of **2**·2EtOH and **2**·2MeOH are obtained and Cu^{2+} centers exhibit a five coordinated square pyramidal geometry with one alcohol coordination (Fig. 3c and d). The crystallization process and subsequent single crystal structure refinement of **1** were more readily obtained than those of **2**, indicating a more stable crystalline packing in the hydrogen bond associated forms of **1**.

The Hirshfeld surface (HS) analysis[34,35] clearly suggests strong hydrogen bonds between the solvated molecules in the crystal of **1**·2EtOH·2H_2O and **1**·8MeOH (Fig. S5–S12†). HS analysis of each MeOH molecule mapped with d_{norm} (the normalized contact distance, defined in terms of d_e, d_i, and the vdW radii of the atoms) and the corresponding fingerprint plots of **1**·8MeOH are shown in Fig. 4. The red spots shown in Fig. 4a are distances remarkably shorter than sum of vdW radii for O(inside)···H(outside)/H(inside)

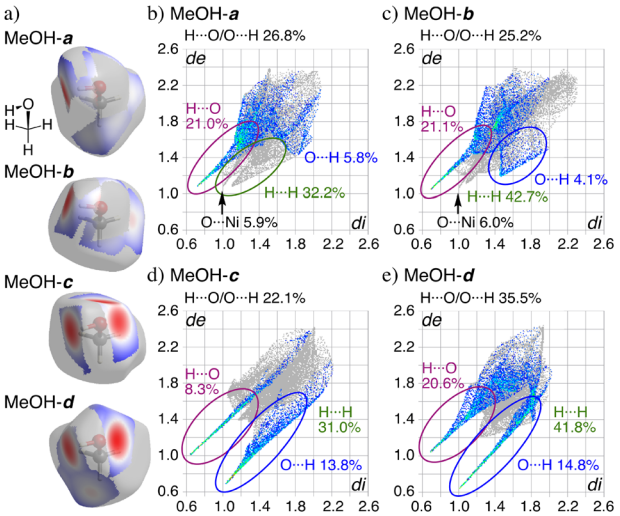

Fig. 4 a) The Hirshfeld surfaces for each MeOH (d_{norm} is a normalized contact distance)[34] and b–e) comparison between the fingerprint plots for MeOH of **1**·8MeOH showing d_e and d_i of 0.6–2.6 Å for all atoms.

···O(outside),[34] indicating the position of intra- and intermolecular hydrogen bonds. The contributions of O···H/H···O to the total interactions for each MeOH are 26.8%, 25.2%, 22.1%, 35.5% in **1**·8MeOH (Fig. 4b). For MeOH-***c***, three specific and sharp hydrogen bonds were characterized as H6···O7 (8.3%) and O6···H4^{i} and O6···H5 (13.8%) without any intermolecular interaction in the region of 1.4 Å around the molecule. The sharp peaks of H(inside)···O(outside) for MeOH-***c*** and O(inside)···H(outside) of MeOH-***d*** shows the same hydrogen bond to form the tetramer. The detailed HS and PLATON analyses suggest that significant interactions between the π-hole of the pentafluorophenyl group and the oxygen atom in MeOH were not observed, as hydrogen bond formation within the coordination pockets was prioritized instead.

Non-solvated **1** was obtained as a brown powder by heating **1**·8MeOH at 110 °C for 2 h under vacuum conditions (Fig. 5a). The brown powder **1** slowly changes to a light green color under exposure to vapors of MeOH, EtOH, and air.

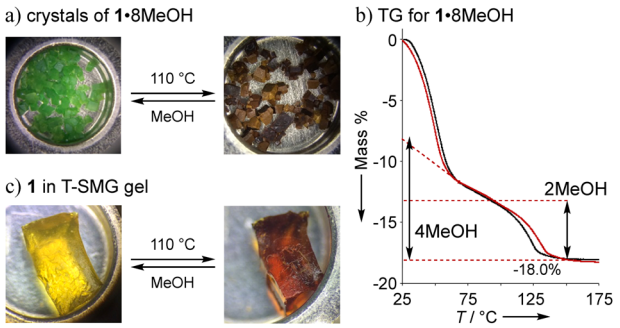

Fig. 5 a) The appearances and b) TG studies of the reversible guest insertion-release processes for **1**·8MeOH: TGA shows 7MeOH; the scanning rate of 5 °C min^{-1}. c) Reversible color change of the T-SMG gel with **1** by MeOH.

Color changes were reversibly observed with good reproducibility through the formation of coordination bonds between the lone pair of guests and the axial positions of Ni^{2+}. The guest insertion/release process is illustrated in Scheme 2, indicating the four-types of guest inserted structures; types-A and B were generally found for **2** and **1** with saturated coordination geometries of square-pyramidal Cu^{2+} ions and octahedral Ni^{2+} ions, respectively; types-C and D are guest inserted structures with guest insertion enhanced through intermolecular hydrogen bonds. Types-C and D are new types of solvated structures and found only in crystals of **1**·8MeOH. To understand the decomposition process and stability of the hydrogen bonds, we performed thermogravimetric analysis (TGA). The results of TGA in air condition of **1** show two H_2O insertions into the crystal (type-A) and the results of elemental analysis in air condition shows **1**·2H_2O: calcd for $C_{34}H_8Ni_2F_{20}O_8$ (%): C 39.20, H 0.77; found: C 39.18, H 0.91. No deliquescence or hygroscopicity was observed for **1** and **2**.

The TGA results of crystal **1**·8MeOH show the existence of intermediate clusters as shown in Fig. 5b. Because MeOH can easily evaporate from the crystals at room temperature, it was not possible to easily distinguish MeOH on the surface of the crystals from MeOH inside the crystals. For this reason, the surface of the crystal was wiped and dried at room temperature immediately after removal from the solvent prior to TGA measurement to show well reproducible desorption amounts (red and black lines); the total elimination of MeOH was found to be −18.0% at 150 °C, close to the calculated value of 18.2% for **1**·7MeOH. The elimination process showed two steps; the results indicate that a certain amount of MeOH is removed at r.t. before the measurement, then the remaining amount of MeOH is quickly released in the 1st step around 60 °C. The remaining MeOH is gradually released at high temperature in the 2nd step, which is also reproducible. More than two molecules up to an equivalent of 4 MeOH given that it is slowly removed from room temperature indicates type-B packing. However, type-A, which is rarely found for **1** (but commonly observed for **2**), cannot be ignored as cross-linking the solvate between two Ni^{2+} ions in crystalline states is possible. Thus, we applied the vapor adsorption/desorption for the crystals as described below.

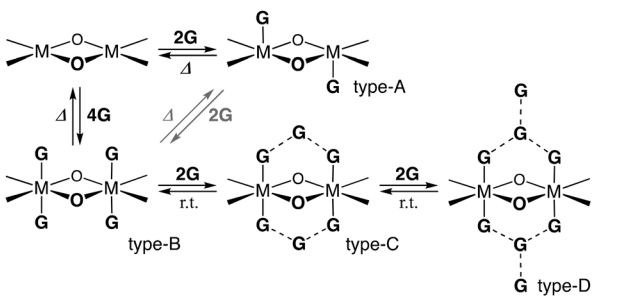

Scheme 2 Four-types of the guest inserted structures of dinuclear metal complexes (M = Ni^{2+} or Cu^{2+}).

The adsorption/desorption isotherms of the complexes **1** and **2** were examined on microcrystalline powder samples, which were activated by heating at 60 °C for 3 h under vacuum condition.[36] The studies of adsorption/desorption of MeOH vapor for the powders of **1** and **2** clearly show two important points: (a) the inserted numbers are highly enhanced for **1** and (b) stepwise desorption process of **1** clearly suggested the existence of types-B and C, indicating that the unique intermolecular hydrogen bonded clusters for **1** were reversibly observed in the solid states. For Fig. 6a, two MeOH molecules are quickly inserted with a type-I isotherm under 0.05 P/P_0 (43 $cm^3\ g^{-1}$). The amount of MeOH is slightly increased around 0.70 P/P_0 (6.4 mol mol^{-1}, 142 $cm^3\ g^{-1}$) and is highly accelerated to give high-solvated crystals with an estimated 38 molecules of MeOH (857 $cm^3\ g^{-1}$ at 0.98 P/P_0). The results show the enhanced adsorption of MeOH through uniform hydrogen bonds between MeOH molecules. The desorption isotherm of **1**·38MeOH shows a unique hysteresis and stepwise release to clearly show that **1**·6MeOH (type-C) gives **1**·4MeOH (type-B) around 0.3–0.2 P/P_0 and **1**·4MeOH (type-B) gives **1** under 0.08 P/P_0 (87 $cm^3\ g^{-1}$). On the other hand, the corresponding complex **2** and MeOH shows a remarkable and reversible guest insertion/release process with type-III isotherms and the maximum numbers are two to give **2**·2MeOH at 0.99 P/P_0 (1.9 mol mol^{-1}, 43 $cm^3\ g^{-1}$), indicating good agreement with the crystal structure (Fig. 3d). Interestingly, the adsorption/desorption isotherms of EtOH and H_2O vapors for the complexes show a low adsorption amount (Fig. 6b and c). In this case, two EtOH molecules are also inserted with a type-I isotherm until 0.05 P/P_0 (44 $cm^3\ g^{-1}$). Since the EtOH adsorption is not hindered by H_2O, the amount slowly increased until 0.80 P/P_0 (6.5 mol mol^{-1}, 146 $cm^3\ g^{-1}$) and finally give **1**·22EtOH at 0.98 P/P_0 (489 $cm^3\ g^{-1}$). The desorption isotherm again shows hysteresis over a wide range, suggesting the formation of **1**·6EtOH (type-C). The result indicates that EtOH behaves like MeOH in the absence of water. For H_2O adsorption, two molecules are inserted with the same isotherm until 0.18 P/P_0 (44 $cm^3\ g^{-1}$), and the amount slowly increased until 0.81 P/P_0 (3.9 mol mol^{-1}, 88 $cm^3\ g^{-1}$) and finally gives **1**·6H_2O at 0.99 P/P_0 (134 $cm^3\ g^{-1}$). The desorption isotherm slowly decreased with hysteresis.[37] Complex **2** shows the formation of **2**·2EtOH (2.3 mol mol^{-1}, 52 $cm^3\ g^{-1}$ at 0.98 P/P_0) and no adsorption of H_2O (0.3 mol mol^{-1}, 5.7 $cm^3\ g^{-1}$ at 0.98 P/P_0).

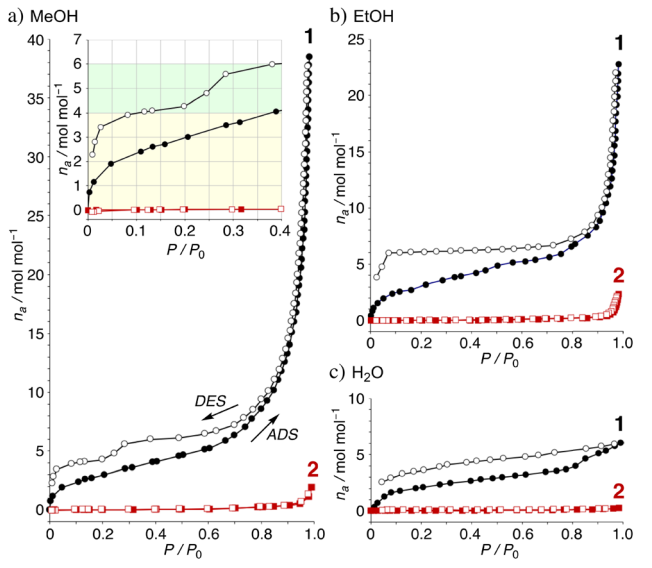

Fig. 6 Adsorption isotherms at 298 K of the complexes (a) MeOH with an inset showing the magnified view at low relative pressures, (b) EtOH, and (c) H_2O: adsorption isotherms at 298 K of the complexes: **1**, black circles; **2**, red squares; filled, adsorption; and open, desorption.

Since we observed color changes in different crystalline states of **1**, we considered confining the complex **1** in a T-SMG gel network,[27] which forms a soft and loose network and allows the complex to be incorporated within. When the gel was then immersed in a $CHCl_3$ solution of **1** at 55 °C for 3 hours, the colorless gel became yellowish green due to incorporation of **1**. The same gel was also obtained by a one-pot photopolymerization synthesis with the reagents and **1** (Fig. S14–S17†). After drying the gel by heating at 110 °C in TGA or vacuum conditions at 60 °C, the color changed to brown, as shown in Fig. 5c. When the brown gel was placed in MeOH vapor, the color became lighter and a swollen yellow green gel was obtained. The color gradually turned yellowish green when exposed to air due to moisture sensitivity. A similar change was observed for the brown gel under the same conditions. From these results, we conclude that the brown gel contains solvent-free **1**, which absorbs alcohol and/or H_2O in the air and shows swelling due to MeOH adsorption. This color change was reversible, and the high transparency of the gel was maintained even after repeating. No corresponding gel with **2** was obtained by the same protocols because of the unexpected reaction of Cu^{2+} and T-SMG gels.

In summary, we demonstrate the enhanced and accelerated MeOH encapsulation and coordination geometry dependant color change using the perfluorinated dinuclear Ni^{2+} complex **1** through the formation of unique and extend hydrogen bonded clusters. No enhanced guest encapsulation behaviors were found for **2**. MeOH clusters are well known to form infinite hydrogen bonds to give zigzag chains at −110 °C and the chains are broken up to small linear and/or cyclic $(MeOH)_n$ (n = 3–20) oligomers above its melting point.[38] While there are a few examples of cyclic MeOH hexamers, first reported in 1962,[39] and subsequently confirmed by crystallographic studies,[40,41] tetrameric MeOH clusters have not been reported except for a single tetrameric MeOH observed in the vapor phase reported in 1951.[42] The crystallographic and adsorption studies of these remarkable MeOH clusters clarify the existence of the tetramer conformation and explain that the centrally present MeOH-***c*** triggers further self-assembly by attracting MeOH to the outside of the complex. Notably, in this complex with a highly uniform cavity on the axial sites of Ni^{2+} ions, the uptake of EtOH is suppressed and stabilized by co-crystallization with H_2O through hydrogen bonds. The high

adsorptivity of MeOH under low pressure is also noteworthy in comparison with guest insertion of EtOH or H_2O. The important results are; (1) the branched tetrameric cluster (type-D) of MeOH was crystallographically found for the first time; (2) the cluster-type intermediate structures (type-C) were observed in the elimination process of gas adsorption only for **1**; (3) the adsorption amount of EtOH and H_2O is less than that of MeOH, and the coordination of each component is rather inhibited in the crystallization process; and (4) the number of crystal solvents and the maximum adsorptions in **2** matched to two molecules, indicating the specificity of the Ni^{2+} complex **1**. Because MeOH stands in the middle of EtOH and H_2O in terms of polarity, size, and hydrogen bond formation, it is important to develop appropriate materials for MeOH for its separation and sensor development. Separation from mixtures and performance in dispersed systems are expected to be further developed.

Conflicts of interest

There are no conflicts to declare.

Acknowledgements

This work was supported by Grant-in-Aids for Scientific Research C (no. 18K05153) and B (21H01955) of JSPS KAKENHI.

Notes and references

1 *Crystal Design: Structure and Function*, ed. G. R. Desiraju, Perspectives in Supramolecular Chemistry, Wiley, 2003.
2 J.-R. Li, R. J. Kuppler and H.-C. Zhou, *Chem. Soc. Rev.*, 2009, **38**, 1477–1504.
3 (*a*) M. Fujita, M. Tominaga, A. Hori and B. Therrien, *Acc. Chem. Res.*, 2005, **38**, 371–380; (*b*) M. Kawano and M. Fujita, *Coord. Chem. Rev.*, 2007, **251**, 2592–2605.
4 (*a*) S. Kitagawa, R. Kitaura and S. Noro, *Angew. Chem., Int. Ed.*, 2004, **43**, 2334–2375; (*b*) J. L. C. Rowsell and O. M. Yaghi, *Microporous Mater.*, 2004, **73**, 3–14; (*c*) H.-S. Choi and M. P. Suh, *Angew. Chem., Int. Ed.*, 2009, **48**, 6865–6869.
5 L. M. Salonen, M. Ellermann and F. Diederich, *Angew. Chem., Int. Ed.*, 2011, **50**, 4808–4842.
6 H. Wang, W. Wang and W. J. Jin, *Chem. Rev.*, 2016, **116**, 5072–5104.
7 (*a*) J. H. Williams, *Crystal Engineering: How Molecules Build Solids*, Morgan & Claypool Publishers, 2017; (*b*) J. H. Williams, *Acc. Chem. Res.*, 1993, **26**, 593–598.
8 K. Shimizu, M. F. C. Gomes, A. A. H. Pádua, L. P. N. Rebelo and J. N. C. Lopes, *J. Phys. Chem. B*, 2009, **113**, 9894–9900.
9 R. J. Doerksen and A. J. Thakkar, *J. Phys. Chem. A*, 1999, **103**, 10009–10014.
10 S. Kundu, B. Sk, P. Pallavi, A. Giri and A. Patra, *Chem. – Eur. J.*, 2020, **26**, 5557–5582.
11 M. Kawano and M. Fujita, *Coord. Chem. Rev.*, 2007, **251**, 2592–2605.
12 K. Nakajima and A. Hori, *Cryst. Growth Des.*, 2014, **14**, 3169–3173.
13 (*a*) A. Hori, in *The importance of π-interactions in crystal engineering*, ed. E. R. Tiekink and J. Zukerman-Schpector, Wiley & Sons, 2012, pp. 163–185; (*b*) A. Hori and T. Arii, *CrystEngComm*, 2007, **9**, 215–217.
14 A. Hori, K. Nakajima, Y. Akimoto, K. Naganuma and H. Yuge, *CrystEngComm*, 2014, **16**, 8805–8817.
15 Y. Ikumura, Y. Habuka, S. Sakai, T. Shinohara, H. Yuge, I. I. Rzeznicka and A. Hori, *Chem. – Eur. J.*, 2020, **26**, 5051–5060.
16 M. Egli and S. Sarkhel, *Acc. Chem. Res.*, 2007, **40**, 197–205.
17 Ç. A. Demircan and U. Bozkaya, *J. Phys. Chem. A*, 2017, **121**, 6500–6509.
18 H. Wang, W. Wang and W. J. Jin, *Chem. Rev.*, 2016, **116**, 5072–5104.
19 X. Pang, H. Wang, W. Wang and W. J. Jin, *Cryst. Growth Des.*, 2015, **15**, 4938–4945.
20 A. V. Rozhkov, M. A. Krykova, D. M. Ivanov, A. S. Novikov, A. A. Sinelshchikova, M. V. Volostnykh, M. A. Konovalov, M. S. Grigoriev, Y. G. Gorbunova and V. Y. Kukushkin, *Angew. Chem., Int. Ed.*, 2019, **58**, 4164–4168; Y. N. Toikka, A. S. Mikherdov, D. M. Ivanov, T. J. Mooibroek, N. A. Bokach and V. Y. Kukushkin, *Cryst. Growth Des.*, 2020, **20**, 4783–4793.
21 E. Fiedler, G. Grossmann, D. B. Kersebohm, G. Weiss and C. Witte, *Methanol, Ullmann's Encyclopedia of Industrial Chemistry*, Weinheim Wiley-VCH, 2005.
22 J. Ozaki, S. K. I. Djaja and A. Oya, *Ind. Eng. Chem. Res.*, 2000, **39**, 245–249.
23 L. Lin, W. Zhou, R. Gao, S. Yao, X. Zhang, W. Xu, S. Zheng, Z. Jiang, Q. Yu, Y.-W. Li, C. Shi, X.-D. Wen and D. Ma, *Nature*, 2017, **544**, 80–83.
24 D. G. Barceloux, G. R. Bond, E. P. Krenzelok, H. Cooper and J. A. Vale, *J. Toxicol., Clin. Toxicol.*, 2002, **40**, 415–446.
25 J. van den Broek, S. Abegg, S. E. Pratsinis and A. T. Güntner, *Nat. Commun.*, 2019, **10**, 4220.
26 T. Kusakawa, S. Sakai, K. Nakajima, H. Yuge, I. I. Rzeznicka and A. Hori, *Crystals*, 2019, **9**, 175.
27 J. Gong, Y. Watanabe, Y. Watanabe, R. Hidema, M. H. Kabir and H. Furukawa, *J. Solid Mech. Mater. Eng.*, 2013, **7**, 455–462.
28 Y. Wang, J. Gong and W. Hu, *Chin. J. Polym. Sci.*, 2020, **38**, 1374–1381.
29 Y. Mao, T. Miyazaki, K. Sakai, J. Gong, M. Zhu and H. Ito, *Polymer*, 2018, **10**, 1117.
30 CSD was released as CSD2022.2.0 on September, 2022.
31 (*a*) $[C_{16}H_2I_8NiO_8{\cdot}4(CH_4O)]{\cdot}2(CH_4O)$: J. Qin, S.-C. Chen, Z.-H. Zhang, F.-A. Sun, W.-Y. Zhou, M.-Y. He and Q. Chen, *J. Chem. Res.*, 2012, **36**, 516–519; (*b*) $[C_{30}H_{28}N_2NiO_4{\cdot}4(CH_4O)]{\cdot}2(CH_4O)$: M. Gacki, K. Kafarska, A. Pietrzak, I. Korona-Głowniak and W. M. Wolf, *Molecules*, 2020, **25**, 3099.
32 $[C_{36}H_{24}N_6O_6{\cdot}Ni(CH_4O)_6]{\cdot}3(CH_4O)$ of CCDC173041: D. M. L. Goodgame, D. A. Grachvogel and D. J. Williams, *Inorganica Chim. Acta*, 2002, **330**, 13–16.
33 (*a*) $[C_{16}H_2CuI_8O_8{\cdot}4(CH_4O)]{\cdot}2(CH_4O)$ of CCDC879565: S.-C. Chen, J. Qin, Z.-H. Zhang, M. Hu, F.-A. Sun, L. Liu, M.-Y. He and Q. Chen, *J. Coord. Chem.*, 2013, **66**, 1924–1932; (*b*) $[C_{40}H_{28}CuO_{10}P_2{\cdot}4(CH_4O)]{\cdot}2(CH_4O){\cdot}H_2O$ of CCDC286358: T. Dorn, A.-C. Chamayou and C. Janiak, *New J. Chem.*, 2006, **30**, 156–167.

34 M. A. Spackman and D. Jayatilaka, *CrystEngComm*, 2009, **11**, 19–32.
35 M. J. Turner, J. J. McKinnon, S. K. Wolff, D. J. Grimwood, P. R. Spackman, D. Jayatilaka and M. A. Spackman, *CrystalExplorer 17*, 2017.
36 (*a*) A. Hori, R. Gonda and I. I. Rzeznicka, *CrystEngComm*, 2017, **19**, 6263–6266; (*b*) R. Gonda, I. I. Rzeznicka, Y. Kinoshita, S. Uchida and A. Hori, *Dalton Trans.*, 2019, **48**, 9062–9066.
37 Since the solubility of **1** in water is extremely low, no comparative experiment of the crystallization from an aqueous solution has been conducted.
38 K. J. Tauer and W. N. Lipscomb, *Acta Crystallogr.*, 1952, **5**, 606.
39 L. Pauling, *The Nature of the Chemical Bond*, Cornell University Press, Ithaca, NY, 1962.
40 L. Benisvy, I. Mutikainen, M. Quesada, U. Turpeinen, P. Gameza and J. Reedijk, *Chem. Commun.*, 2006, 3723–3725.
41 M. Mikuriya, H. Azuma and M. Handa, *Mol. Cryst. Liq. Cryst.*, 2002, **379**, 205–210.
42 W. Weltner and K. S. Pitzer, *J. Am. Chem. Soc.*, 1951, **73**, 2606–2610.

